



Optics Letters

Measuring the shape of microbends in optical fibers

RAJA AHMAD,* WING KO, KENNETH S. FEDER, AND PAUL S. WESTBROOK

OFS Laboratories, 19 Schoolhouse Road, Suite 105, Somerset, New Jersey 08873, USA

*Corresponding author: rahmad@ofsoptics.com

Received 16 March 2020; revised 30 July 2020; accepted 3 August 2020; posted 5 August 2020 (Doc. ID 392366); published 14 September 2020

We report on the distributed shape measurement of small deformations produced along the length of an optical fiber. The fiber contains multiple waveguiding cores, each inscribed with weak continuous Bragg gratings. The distributed Bragg-reflectivity data for the fiber cores, obtained from the optical backscatter reflectometry, are used to estimate the local curvature and the position of the fiber. We successfully demonstrate the sensing of periodic microdeformations—approximately 1 μm or less in amplitude and a few hundred μm in length. Such microbends are known to cause attenuation in optical fibers, and the approach presented here can enable a detailed measurement of these microbends in applications ranging from telecommunications cable design to biotechnology, robotics, manufacturing, aerospace, and security. © 2020 Optical Society of America

<https://doi.org/10.1364/OL.392366>

The optical fiber distributed sensors have emerged as an invaluable tool for breakthrough scientific studies and for advanced technological developments [1,2]. A few advantages of optical-fiber-based distributed sensors over their electronic, mechanical, or nonguided-wave electromagnetic counterparts include compactness, accuracy, reliability, noninvasiveness, immunity against environmental interference, and intrinsic safety. The exceptional performance of optical fiber distributed temperature, strain, and pressure sensors is widely recognized [1–5], and such sensors have found widespread applications in a variety of fields, such as in energy exploration, aerospace, transportation, and mechanical structure monitoring.

The distributed sensing of arbitrarily deformed paths and shapes presents innumerable potential applications in emerging technologies such as 3D printing, surgical catheters, smart wearables, and monitoring systems for fuel tanks and composite structures [6–11]. The optical fibers for shape sensing offer high-precision and high-speed operation and can be particularly applicable for characterizing difficult-to-access surfaces and environments, owing to the shielded propagation of the probing light [12]. In the past, macroscale distributed sensing with optical fibers has been demonstrated to reconstruct arbitrary paths and shapes [13–16]. Distributed shape sensing at smaller-length scales carries great potential rewards for

applications where high sensitivity, resolution, and precision are indispensable features. In particular, the influence of fiber microbends on the attenuation in optical fibers has been of interest for several decades [17–23]. As the transmission loss in optical fibers approaches the fundamental limits dictated by the intrinsic absorption and scattering in glass, the losses induced by the microscopic physical bends in the optical fibers and cables are becoming increasingly relevant. However, such microbends cannot be measured directly with current methods. This introduces a demand for tools that are capable of detecting and characterizing the local microdeformations in optical fibers.

In this Letter, we present the reconstruction of the microdeformations that are distributed along the length of an optical fiber. The sensing scheme is based on probing the distributed reflection of light within the waveguiding cores that are symmetrically situated at a fixed radial offset from the central axis of the twisted multicore fiber. The reflection of the light is facilitated by continuous fiber Bragg gratings (FBGs) that are UV-inscribed in each of the offset cores. A microscale deformation, or the microbending, of the fiber locally produces a nonuniform transverse stress, which results in a corresponding local shift in the Bragg wavelength. The distributed Bragg reflection within the various offset cores is then combined to estimate the curvature and the shape of the deformed fiber. We evaluate the performance of our system by applying and detecting periodic fiber deformations, which are in the range of 1 μm in transverse amplitude with longitudinal spatial period of 900–500 μm . This represents a promising scheme for characterizing distributed mechanical deformations with an ultrahigh sensitivity, providing an unprecedented tool for measuring microbends along substantial lengths of fiber with an impact on the cable and fiber design for telecommunications, biomedicine, 3D manufacturing, aerospace, and defense.

Figure 1(a) shows a photograph of the twisted multicore optical fiber's cleaved endface—see Ref. [23] for fiber details. Within the fiber, there are a total of six offset waveguiding cores and one center core, identical in diameter and refractive-index profiles. The offset cores are located at a fixed radial offset $R_0 (= 35 \mu\text{m})$ from the center of the fiber, with an angular offset of 60° among the neighboring cores. The mode field diameter and the numerical aperture of the waveguiding cores is 6 μm and 0.21, respectively, whereas the LP_{11} -mode cutoff wavelength is $< 1310 \text{ nm}$. The overall fiber diameter is 200 μm ,

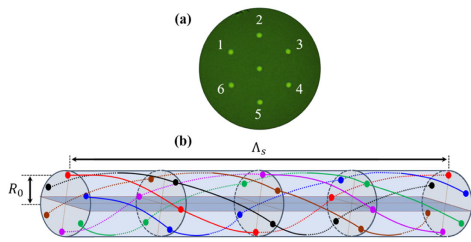


Fig. 1. (a) Microscope image of the cleaved multicore fiber endface and (b) illustration of the twisted waveguiding cores in the fiber.

which includes a silica glass circular region and a protective polymer coating layer that are $62.5 \mu\text{m}$ in radius and $37.5 \mu\text{m}$ in thickness, respectively. During the fiber draw, the preform is continuously rotated, which leads to the offset cores spiraling around the central axis of the fiber at a twist frequency of 50 rotations per meter (spatial twist period $\Lambda_s = 2 \text{ cm}$)—see Fig. 1 (b) for an illustration.

Figure 2(a) shows a simplified schematic diagram of the experimental setup. In the experiment, we demonstrate that the textured hard surfaces (of aluminum plates, in the present case) can be profiled by tracking the deformations in the twisted multicore fiber that is pressed against the surface to mimic its texture. Optical frequency domain reflectometry (OFDR) measurements—operation details to be provided in the next section—are performed on the backscattered signals within the multiple cores of the fiber. After placing the fiber-under-test (FUT) between the pair of aluminum plates, a controlled force is applied to induce the fiber deformations. Physically, the resulting bends along the length of the FUT produce a local asymmetric stress within the fiber cross-section, as depicted in Fig. 2(b). This transverse stress distribution is probed at various locations within the fiber cross-section with the help of the multiple offset cores. The subsequent analysis of the transverse stress profiles at closely spaced positions along the length of the FUT reveals the fiber bending and twist directions as well as the amplitude of the spatially continuous curvature of the bent fiber. This information enables us to perform the full-scale distributed

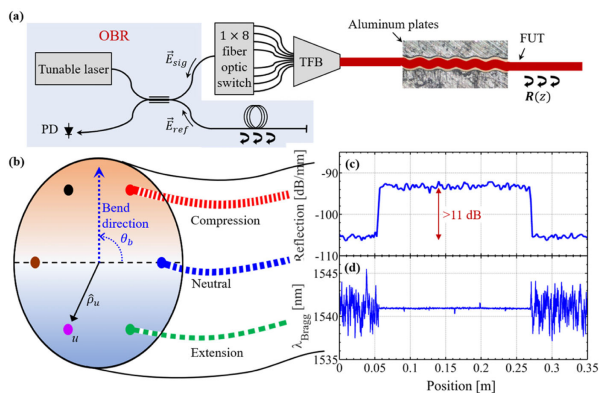


Fig. 2. (a) Experimental setup; PD: photodetector, FUT: fiber-under-test; (b) depiction of the transverse stress within the deformation imposed FUT at a particular position along its length. The bend puts the red core FBG in compression, decreasing its length, and the green core in extension, lowering the period. The blue core is unaffected since it is at the neutral plane of the fiber; center-core (c) reflected signal power and (d) Bragg wavelength along the length of the FUT.

deformations measurement on the bent FUT and, therefore, to estimate the surface profile of the aluminum plates.

In order to improve the signal-to-noise ratio in the OFDR processing, the amount of the reflected signal is enhanced by inscribing weak FBGs within the fiber cores [24]. Figure 2(c) clearly shows an enhancement of the backscattered signal, by more than 11 dB with respect to the background noise, within the FBG inscribed section of the FUT. The background noise represents the Rayleigh backscattering that naturally occurs within the cores of the glass fiber. The waveguiding cores are doped with germanium to facilitate the FBG inscription using a 248 nm wavelength pulsed excimer laser. The polymer coating layer surrounding the silica glass region is UV-transparent, which alleviates the need for the coating removal during the FBG inscription and is, therefore, helpful toward maintaining the fiber strength. As shown in Fig. 2(d), the inscribed continuous FBG is resonant at the wavelength $\lambda_{\text{Bragg}} \sim 1541 \text{ nm}$, which lies within the operation window (1525–1610 nm) of the commercially available OFDR instrument (OBR, LUNA Inc.) used in our experiments.

The local changes in the Bragg wavelengths $\Delta\lambda_{\text{Bragg}}(z) (= \lambda_{\text{Bragg}}(z) - \lambda_{\text{Bragg}})$, computed via the OFDR processing (described in detail in ref. 12), for the six offset cores [as labeled in Fig. 1(a)] are presented in Fig. 3(a), where the aluminum plates have a sinusoidally deformed surface of period $\Lambda_d = 900 \mu\text{m}$. The beat pattern observed in the modulated Bragg wavelength along the length of the offset cores in the periodically bent FUT is a manifestation of the monotonic twisting of the fiber cores. More precisely, the Bragg wavelengths of the offset cores vary in proportion to $\cos(k_s z) * \cos(k_d z)$, where $k_{s(d)} (= 2\pi/\Lambda_{s(d)})$ is the spatial wavenumber of the spiraling offset cores (surface deformations). This is clearly indicated by the spatial Fourier transform of the modulated Bragg wavelengths, as shown in Fig. 2(b), where two main frequency components corresponding to $k_d \pm k_s$ are present. The beat notes in $\Delta\lambda_{\text{Bragg}}(z)$ for the six fiber cores are spatially offset from one another by length $L_{\text{off}} = \frac{\Lambda_s}{3}$ that corresponds to the angular offset $\theta_{\text{off}} = \frac{\pi}{3}$ among the respective cores. It is also worth noting that the spatial resolution of the distributed measurement of the local Bragg wavelengths, and that of the subsequent shape reconstruction, is $\sim 40 \mu\text{m}$. The spatial resolution can be further improved by increasing the wavelength tuning range of the laser for OFDR processing. The OBR laser used in the present setup can be tuned over an 80 nm wavelength span, which would correspond to a spatial resolution of $\sim 10 \mu\text{m}$ for the silica-glass-based optical fibers. Note that inclusion of this extra bandwidth increases the spatial resolution even though the signal reflection is relatively strong near the Bragg wavelength; because of the Fourier relationship, the shorter-length spatial perturbations are manifested in the additional spectrum far from the Bragg wavelength, demanding a broadband OFDR laser scan in order to track these fine-scale axial changes.

Next, we compute the distributed curvature of the FUT upon undergoing the spatially continuous periodic bending between the corrugated aluminum plates. The distributed curvature is a vector quantity, $\vec{\kappa}(z)$, and its phase offers information about the bend direction, thereby enabling us to reconstruct the distributed shape of the fiber. In general, the spatially dependent curvature $\vec{\kappa}(z)$ depends on the local strain and the geometry of a fiber core and is given as [15]

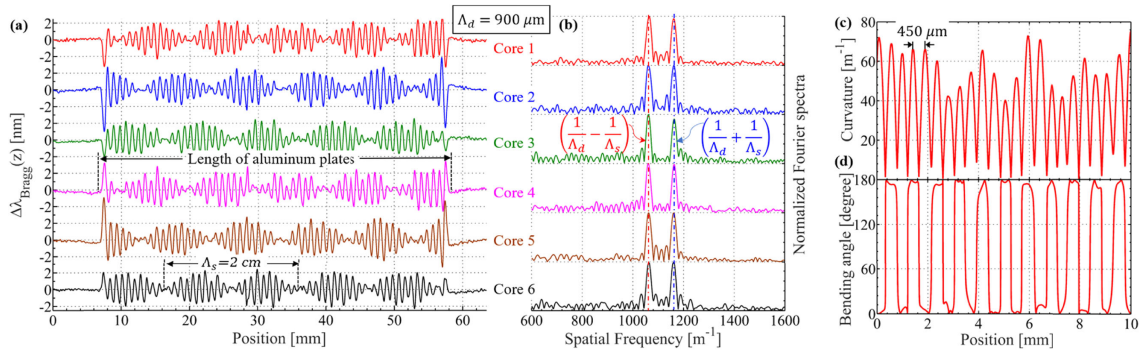


Fig. 3. (a) Position-dependence of the Bragg wavelength in each core of the periodically deformed fiber; (b) Fourier transform of the position-dependent Bragg resonance changes in the corresponding fiber cores; spatially continuous (c) curvature and (d) bend direction of the deformed FUT.

$$\vec{\kappa}(z) = \frac{1}{r} \sum_{u=1}^n \hat{\rho}_u(z) \varepsilon_u(z), \quad (1)$$

where $r (= 35 \mu\text{m})$ is the radial distance between the center of an offset core and the center of the overall fiber, $u = \{1, \dots, n\}$ is a label for the offset core(s) used in the experiment, $\hat{\rho}_u(z)$ is the unit vector of the respective core, as sketched in Fig. 2(a), and ε_u is the strain induced in the corresponding core u . Using the strain-optic coefficient η (~ 0.78) of the silica glass [25] and the measured local changes in the Bragg wavelength $\Delta\lambda_{\text{Bragg}}(z)$, shown in Fig. 3(a), we estimate the corresponding local strain, $\varepsilon_u(z) = \frac{1}{\eta} \frac{\Delta\lambda_{\text{Bragg},u}(z)}{\lambda_{\text{Bragg}}}$, experienced by the offset core u within the FUT. While the strain and position information for a single offset twisted core is mathematically sufficient for the measurement of fiber curvature using Eq. (1), the sensitivity to fabrication and OBR measurement errors in an individual core can be minimized by including information from the multiple offset cores. Therefore, we combine the strain information from six offset cores, which are disposed along twisted paths within the FUT and are, at any position along the fiber length, angularly offset from one another by precisely 60° ($\pi/3$ radians) within the fiber cross-section. Figures 3(c) and 3(d) show, respectively, the magnitude and the phase of the distributed fiber curvature, computed via the Eq. (1). The monotonically varying data plot in Fig. 3(c) shows that the curvature produced in the FUT can be monitored with a high precision and spatial resolution. It is worth noting that the fiber curvature approaches zero twice within one period of the sinusoidally deformed FUT. These locations correspond to the zero-crossing points of a pure sinusoid, where the slope of the curve is strictly linear, and, hence, no strain is produced within the fiber cross-section at such locations. Moreover, the bend orientation of the FUT points in opposite directions around each zero-curvature location. This is also indicated in Fig. 3(d), which shows that the phase component of the fiber curvature, $\theta_b(z) (= \angle \vec{\kappa}(z))$, which represents the bend direction of the periodically deformed fiber, continuously changes by $\pm 180^\circ$ (π radians) at the zero-curvature locations. The 180° changes in $\vec{\kappa}(z)$ match the vertical direction of the microbend deformation precisely without any calibration, giving a strong confirmation of the shape-sensing capability of our fiber even with very small deformations of the fiber. We also note that, because of the twisted outer cores, our sensor is equally sensitive to transverse deformations from any azimuthal angle.

Finally, the distributed shape of the deformed fiber is reconstructed by using the Frenet–Serret formulas, which are a set of differential equations describing a 3D curve. Specifically, the Frenet–Serret equations relate the local shape parameters, including the tangent $\mathbf{T}(x, y, z)$, normal $\mathbf{N}(x, y, z)$, and binormal $\mathbf{B}(x, y, z)$ vectors, with the fiber curvature and torsion measured at the closely spaced locations. Mathematically, we may write

$$\dot{\mathbf{S}} = \begin{bmatrix} 0 & \kappa(z) & 0 \\ -\kappa(z) & 0 & \tau(z) \\ 0 & -\tau(z) & 0 \end{bmatrix} \mathbf{S}, \quad (2)$$

where $\mathbf{S} \equiv [\mathbf{T}(x, y, z); \mathbf{N}(x, y, z); \mathbf{B}(x, y, z)]$, $\dot{\mathbf{S}} = d\mathbf{S}/dz$, and the torsion $\tau(z)$ quantifies how rapidly the bend direction changes along the length of the curved fiber. In practice, a spatial derivative of the phase component of the distributed curvature vector leads to the amount of torsion $\tau(z) (= d\theta_b(z)/dz)$ produced along the length of the FUT. By repeatedly solving Eq. (2) for the eigenvalues and eigenvectors of the set \mathbf{S} along the length (z axis) of the FUT, we estimate the distributed shape of the fiber. It is important to note that the initial conditions for solving Eq. (2) assume an absence of curvature and torsion at the location $z = 0$ i.e., $\kappa(0) = \tau(0) = 0$. Furthermore, the tangent $\mathbf{T}(x, y, z)$, normal $\mathbf{N}(x, y, z)$, and binormal $\mathbf{B}(x, y, z)$ vectors, at $z = 0$, are defined as the three orthonormal unit vectors in an arbitrarily chosen 3D spatial frame-of-reference. The tangent vector at any position is assumed to be “pointing” in the direction of the increasing fiber length and indicates the local fiber direction. Therefore, a concatenation of the tangent vectors at closely spaced locations along the length of the FUT represents the distributed shape of the fiber. In Fig. 4(a), we show the reconstructed shape of the FUT pressed between the pair of aluminum plates with periodic surface deformations of period $\Lambda_d = 900 \mu\text{m}$. The reconstruction of the distributed shape of the FUT may serve as a proxy for profiling the surface deformations on the aluminum plates. It is worth noting that the distributed shape of the fiber can be tracked with a spatial resolution that is submicrometer in the transverse plane and is $\sim 40 \mu\text{m}$ (limited by the scanning range of the OBR laser) along the longitudinal axis. To further evaluate the performance of our fiber for the surface profiling and distributed shape reconstruction, we carried out similar measurements for aluminum plates with surface deformations of various spatial periods. Figures 4(b) and 4(c) illustrate the reconstructed shape of the

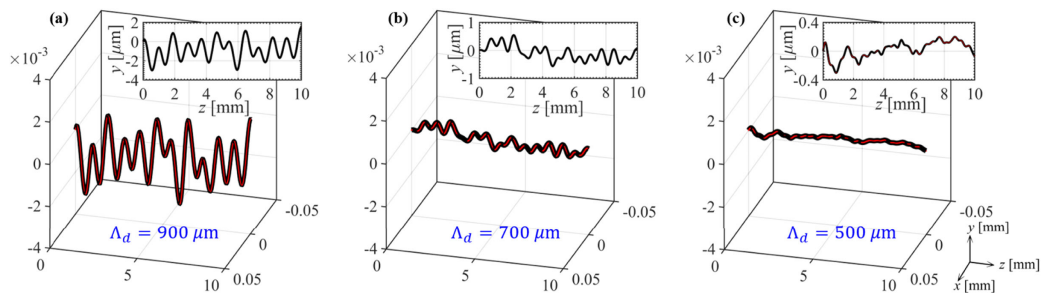


Fig. 4. Reconstruction of the path followed by the fiber under the influence of microdeformations, of period Λ_d (a) 900 μm , (b) 700 μm and (c) 500 μm , imposed by a force of ~ 1 N/mm along the corrugations shown in Fig. 2(a); (insets) the shape of the deformed fiber in the y - z plane.

FUT with imposed deformations of period $\Lambda_d = 700$ μm and 500 μm , respectively, using a 5 kg load distributed over a 5 cm length of the FUT. As shown in the inset of Fig. 4(b), we find that the transverse displacement of the fiber by less than 1 μm with respect to a nondeformed, neutral axis can be tracked. The accuracy of the measurements for the case of $\Lambda_d = 500$ μm suffers from the Bragg wavelength shift $\Delta\lambda_{\text{Bragg}}(z)$ that is barely above the OBR noise floor due to the ultra-small transverse fiber deformations (theoretical estimate: $\sim 0.16\mu\text{m}$, for an applied force ~ 1.08 N/mm and a fiber diameter 125 μm [12]). It is worth mentioning that the OBR instrument noise affects the local measurements of fiber deformation along x and y axes on a similar scale. For potential improvements in the future, we note that the measurement sensitivity determining the smallest detectable transverse fiber deformations can be further improved by (1) increasing the signal-to-noise ratio of the OFDR instrument for the backscattered signals, (2) increasing the precision of the measured backscattered signal, which can be accomplished by an improvement in the accuracy and resolution of both the scanning laser wavelength tuning and the OBR return loss, (3) increasing the radial offset R_0 between the twisted cores and the central axis of the fiber while maintaining the overall fiber (glass) diameter, (4) reducing the fiber diameter to lower the moment of inertia of the cylindrical fiber, and/or (5) using a waveguide material with a higher strain-optic response η with respect to the silica glass. On the other hand, the longitudinal sensitivity of the measurements can be enhanced by increasing the precision of the estimated group delay for the distributed backscattered signal.

In summary, we present a high-resolution characterization of the shape of microbends produced in a twisted multicore optical fiber using the corrugated metal surfaces. The fiber cores are inscribed with weak, continuous Bragg gratings to enhance the backscattered signals for OFDR signal processing. The data from the six offset waveguiding cores is used to obtain strain information within the fiber cross-section, which enables us to track the shape of the deformed fiber being pressed against the metal surface. The transverse fiber deformations in the order of 1 μm are successfully tracked, whereas a longitudinal spatial resolution of ~ 40 μm is achieved for the 20 nm wavelength scanning range of the laser used for swept wavelength interferometry in the OFDR. These results present an attractive path toward developing advanced tools for high-density fiber cables

and aerospace, biotechnology, robotics, and automotive industries to characterize complicated and obstructed paths, shapes and surfaces.

Disclosures. The authors declare no conflicts of interest.

REFERENCES

- P. Lu, N. Lalam, M. Badar, B. Liu, B. T. Chorpeneing, M. P. Buric, and P. R. Ohodnicki, *Appl. Phys. Rev.* **6**, 041302 (2019), and references therein.
- L. S. Grattan and B. T. Meggitt, eds., *Optical Fiber Sensor Technology: Advanced Applications-Bragg Gratings and Distributed Sensors* (Springer, 2013).
- X. Bao and L. Chen, *Sensors* **12**, 8601 (2012).
- G. B. Hocker, *Appl. Opt.* **18**, 1445 (1979).
- L. Thevenaz, M. Nikles, A. Fellay, M. Facchini, and P. A. Robert, *Proc. SPIE* **3330**, 301 (1998).
- J. Kim, A. S. Campbell, B. Esteban-Fernández de Ávila, and J. Wang, *Nat. Biotechnol.* **37**, 389 (2019).
- B. Massaroni, P. Saccomandi, and E. Schena, *J. Funct. Biomater.* **6**, 204 (2015).
- R. Di Sante, *Sensors* **15**, 18666 (2015).
- A. Barrias, J. R. Casas, and S. Villalba, *Sensors* **16**, 748 (2016).
- L. Schenato, *Appl. Sci.* **7**, 896 (2017).
- K. Feng, J. Cui, H. Dang, H. Zhang, S. Zhao, and J. Tan, *IEEE Photon. Technol. Lett.* **28**, 2339 (2016).
- R. Ahmad, P. S. Westbrook, W. Ko, and K. S. Feder, *APL Photon.* **4**, 066101 (2019).
- R. G. Duncan, M. E. Froggatt, S. T. Kreger, R. J. Seeley, D. K. Gifford, A. K. Sang, and M. S. Wolfe, *Proc. SPIE* **6530**, 65301S (2007).
- C. G. Askins, G. A. Miller, and E. J. Friebele, in *Conference on Optical Fiber Communication/National Fiber Optic Engineers Conference* (2008), paper OMT3.
- J. P. Moore and M. D. Rogge, *Opt. Express* **20**, 2967 (2012).
- Z. Zhao, M. A. Soto, M. Tang, and L. Thévenaz, *Opt. Express* **24**, 25211 (2016).
- W. B. Gardner, *Bell Syst. Tech. J.* **54**, 457 (1975).
- D. Marcuse, *Bell Syst. Tech. J.* **55**, 937 (1976).
- D. Marcuse, *Appl. Opt.* **23**, 1082 (1984).
- A. Bjarklev, *J. Lightwave Technol.* **4**, 341 (1986).
- M. D. Rourke, *Opt. Lett.* **6**, 440 (1981).
- C. Unger and W. Stocklein, *J. Lightwave Technol.* **12**, 591 (1994).
- X. Jin and F. P. Payne, *J. Lightwave Technol.* **34**, 1247 (2016).
- P. S. Westbrook, T. Kremp, K. S. Feder, W. Ko, E. M. Monberg, H. Wu, D. A. Simoff, T. F. Taunay, and R. M. Ortiz, *J. Lightwave Technol.* **35**, 1248 (2017).
- K. O. Hill and G. Meltz, *J. Lightwave Technol.* **15**, 1263 (1997).